EURASIP Journal on Applied Signal Processing 2005:3, 296–305

Influence of the Antennas on the Ultra-Wideband Transmission

Werner Sörgel
Institut für Höchstfrequenztechnik und Elektronik, Universität Karlsruhe (TH), Kaiserstrasse 12, 76128 Karlsruhe, Germany
Email: werner.soergel@ihe.uka.de

Werner Wiesbeck
Institut für Höchstfrequenztechnik und Elektronik, Universität Karlsruhe (TH), Kaiserstrasse 12, 76128 Karlsruhe, Germany
Email: werner.wiesbeck@ihe.uka.de

Received 29 October 2003; Revised 16 February 2004

Spectrum is presently one of the most valuable goods worldwide as the demand is permanently increasing and it can be traded only locally. Since the United States Federal Communications Commission (FCC) has opened the spectrum from 3.1 GHz to 10.6 GHz, that is, a bandwidth of 7.5 GHz, for unlicensed use with up to −41.25 dBm/MHz EIRP, numerous applications in communications and sensor areas are showing up. Like all wireless devices, these have an antenna as an integral part of the air interface. The antennas are modeled as linear time-invariant (LTI) systems with a transfer function. The measurement of the antenna's frequency-dependent directional transfer function is described. Quality measures for the antennas like the peak value of the transient response, its width and ringing, as well as the transient gain are discussed. The application of these quality measures is shown for measurements of different UWB antennas.

Keywords and phrases: ultra-wideband, ultra-wideband antennas, quality measures for UWB antennas, time-domain antenna characterization, transient radiation and reception.

1. INTRODUCTION

In April 2002, the Federal Communications Comission (FCC) has released the first report and order regarding the application of ultra-wideband (UWB) communication devices [1]. The antennas are an essential part of such systems as of any wireless system. All antenna's properties depend strongly on the frequency. Therefore, the transmitted waveform is filtered by the antenna structure. The ultra-wide bandwidth allows for resolving the fine structure of the transient transmitting and receiving performance of the antenna. For the free-space propagation channel, the channel impulse response depends only on the antennas' filtering characteristic. In the case of a line-of-sight (LOS) channel, the energy content of the channel impulse response is dominated by the direct path, which again is filtered by the transient responses of the employed antennas. For the analysis of environments with the condition of rich multipath like non-line-of-sight (NLOS), one has to take into account that the filtering characteristic of the antenna has not only an impact on the frequency domain and the time domain but has also a spatial component. This results in different filtering characteristics for different directions and leads to a weighted excitation of the different paths. Therefore, the theoretical analysis and the experimental verification of the spatio-temporal characteristics of UWB antennas are an important issue for the design of UWB systems.

2. UWB ANTENNA MODEL

In general, the electrical properties of antennas are characterized by input impedance, efficiency, gain, effective area, radiation pattern, and polarization properties [2, 3, 4]. For narrowband applications, it is possible to analyze these at the center frequency of the system. For wider bandwidths, the parameters become strongly frequency dependent. The straightforward evaluation of the parameters as functions of frequency is not sufficient for the characterization of the transient radiation behavior. This has to be considered when dealing with UWB modulation schemes like pulse-position modulation, chirp, direct sequence spread spectrum (DSSS), orthogonal frequency division multiplex (OFDM), and the related waveforms.

One proper approach to take into account transient phenomena is to model the antenna as an LTI system [5, 6, 7, 8, 9,

10]. This has to be done for the receiving mode (Section 2.1) and the transmitting mode (Section 2.2). Both systems are related to each other by the reciprocity theorem.

2.1. Transient reception

It is assumed that a plane wave from the direction (Θ_i, ψ_i) with the polarized field strength spectrum $\vec{E}_i$ hits an antenna, which is terminated with its real and frequency-independent characteristic port impedance Z_C. The received voltage spectrum $U_{\mathrm{rx},i}$, which is measured across the terminating load, is a linear combination of the antenna's normalized effective height $\vec{H}_i$ and the incident field (1). In the time domain, this leads to the convolution of two vectors, which is the sum of the convolutions for the two independent polarizations (2):

$$\frac{U_{\mathrm{rx},i}(\omega,\theta_i,\psi_i)}{\sqrt{Z_C}} = \vec{H}_n(\omega,\theta_i,\psi_i)\cdot\frac{\vec{E}_i(\omega,\theta_i,\psi_i)}{\sqrt{Z_0}}, \tag{1}$$

$$\begin{aligned}\frac{u_{\mathrm{rx},i}(t)}{\sqrt{Z_C}} &= \vec{h}_n(t,\theta_i,\psi_i) * \frac{\vec{e}_i(t,\theta_i,\psi_i)}{\sqrt{Z_0}} \\ &= \frac{1}{\sqrt{Z_0}}\left(h_{n,\mathrm{copol}}(t,\theta_i,\psi_i) * e_{i,\mathrm{copol}}(t,\theta_i,\psi_i)\right. \\ &\qquad \left. + h_{n,\mathrm{xpol}}(t,\theta_i,\psi_i) * e_{i,\mathrm{xpol}}(t,\theta_i,\psi_i)\right).\end{aligned} \tag{2}$$

The linearity of the problem allows for the superposition of all incident plane waves. Therefore, the antenna in the receiving mode is fully characterized by its normalized time and angle-dependent transient response $\vec{h}_n(t,\theta,\psi)$ in the time domain or by the corresponding transfer function $H_n(\omega)$ in the frequency domain with the angular frequency $\omega = 2\pi f$. The dimension of $\vec{h}_n$ is m/s. The time-integrating convolution operation $\vec{h}_n *$ yields the unit m. Accordingly, the unit of the transfer function H_n is also m. This is related to the definition of a normalized effective antenna height. It is called normalized due to the termination of the antenna port with the characteristic impedance Z_C. Therefore, losses due mismatch of the feeding network are included in the transient response. This is in contrast to the standard definition of the effective height h, which relates the incident electric field to the antenna's open-circuit voltage.

2.2. Transient radiation

The relationship of the radiated electrical field $\vec{E}_{\mathrm{tx}}$ in a certain distance r and direction (θ,ψ) in the far-field region and the exciting voltage $U_{\mathrm{tx}}(\omega)$ at the connector is modeled as follows:

$$\begin{aligned}\frac{\vec{E}_{\mathrm{tx}}(\omega,r,\theta,\psi)}{\sqrt{Z_0}} &= \frac{1}{r}\exp\left(-j\omega\frac{r}{c_0}\right)\vec{A}_n(\omega,\theta,\psi)\frac{U_{\mathrm{tx}}(\omega)}{\sqrt{Z_C}}, \\ \frac{\vec{e}_{\mathrm{tx}}(t,r,\theta,\psi)}{\sqrt{Z_0}} &= \frac{1}{r}\delta\left(t-\frac{r}{c_0}\right) * \vec{a}_n(t,\theta,\psi) * \frac{u_{\mathrm{tx}}(t)}{\sqrt{Z_C}}.\end{aligned} \tag{3}$$

The transient radiation properties are included in the directional and polarized transmit factors A_n in the frequency domain and a_n in the time domain. Z_0 denotes the characteristic free-space impedance ($Z_0 = 120\pi\Omega$), Z_c is the reference impedance at the antenna connector (assumed to be frequency independent), and r is the distance from the antenna. The convolution with the Dirac function $\delta(t - r/c_0)$ represents the time retardation due to the finite speed of light c_0. The antenna transmit factor depends on the regarded direction (Θ,ψ) of the radiation and is a vector according to the polarization vector properties (copolarization and cross-polarization) of the modeled antenna. The application of the *reciprocity theorem* [5, 9, 10] yields the connection between the receive and transmitting mode in the frequency and in the time domain:

$$\vec{A}_n(\omega,\theta,\psi) = \frac{1}{2\pi c_0} j\omega\vec{H}_n(\omega,\theta,\psi), \tag{4}$$

$$\vec{a}_n(t,\theta,\psi) = \frac{1}{2\pi c_0}\frac{\partial}{\partial t}\vec{h}_n(t,\theta,\psi). \tag{5}$$

Equation (4) leads to the conclusion that an antenna with a finite effective height H_n will not radiate for $\omega = 0$. With (4) and (5), the transient radiation (3) can be rewritten as

$$\frac{\vec{E}_{\mathrm{tx}}(\omega,r,\theta,\psi)}{\sqrt{Z_0}} = \frac{1}{2\pi c_0 r}\exp\left(-j\omega\frac{r}{c_0}\right)j\omega\vec{H}_n(\omega,\theta,\psi)\frac{U_{\mathrm{tx}}(\omega)}{\sqrt{Z_C}}, \tag{6}$$

$$\frac{\vec{e}_{\mathrm{tx}}(t,r,\theta,\psi)}{\sqrt{Z_0}} = \frac{1}{r}\delta\left(t-\frac{r}{c_0}\right) * \frac{1}{2\pi c_0}\frac{\partial}{\partial t}\vec{h}_n(t,\theta,\psi) * \frac{u_{\mathrm{tx}}(t)}{\sqrt{Z_C}}. \tag{7}$$

As the factor $j\omega$ can be placed anywhere in (6), the derivation $\partial/\partial t$ and the convolution $*$ can be exchanged. This results in the known formulation for the radiated fields of impulse radiating antennas (IRAs) [5, 6, 7]:

$$\frac{\vec{e}_{\mathrm{tx}}(t,r,\theta,\psi)}{\sqrt{Z_0}} = \frac{1}{2\pi r c_0}\delta\left(t-\frac{r}{c_0}\right) * \vec{h}_n(t,\theta,\psi) * \frac{\partial}{\partial t}\frac{u_{\mathrm{tx}}(t)}{\sqrt{Z_C}}. \tag{8}$$

It is important to emphasize that the transient response of the antenna $\vec{h}_n$ can introduce any spatio-temporal filter characteristic, which may be far apart from an ideal Dirac pulse which would characterize the transmitting antenna as a mere differentiator in time, as it is very often assumed.

2.3. Free-space UWB transmission

The received voltage of a system consisting of the transmitting antenna 1 and the receiving antenna 2, which are placed in free space and in the mutual far field, can be expressed by combining equations for the frequency domain (1) with (6) and the time domain (2) with (7), respectively:

$$\begin{aligned}U_{\mathrm{rx},2}(\omega) &= \sqrt{\frac{Z_{C,2}}{Z_{C,1}}}\vec{H}_{n,2}(\omega,\theta_i,\psi_i)\frac{\exp\left(-j\omega(r_{12}/c_0)\right)}{2\pi r_{12}c_0} \\ &\quad\cdot j\omega\vec{H}_{n,1}(\omega,\theta_t,\psi_t)U_{\mathrm{tx},1}(\omega),\end{aligned} \tag{9}$$

$$\begin{aligned}u_{\mathrm{rx},2}(t) &= \sqrt{\frac{Z_{C,2}}{Z_{C,1}}}\vec{h}_{n,2}(t,\theta_i,\psi_i) * \frac{1}{2\pi r_{12}c_0}\delta\left(t-\frac{r_{12}}{c_0}\right) \\ &\quad * \vec{h}_{n,1}(t,\theta_t,\psi_t) * \frac{\partial}{\partial t}u_{\mathrm{tx},1}(t).\end{aligned} \tag{10}$$

For the transmitting antenna with the transient response $\vec{h}_{n,1}$, the direction of the receiving antenna is denoted with (θ_t, ψ_t) in the appropriate local coordinate system. For the receiving antenna, the direction of the transmitting antenna is denoted accordingly with (θ_i, ψ_i). In the often encountered case that both antenna transfer functions are normalized to the same characteristic port impedance (e.g., $Z_{C,1} = Z_{C,2} = 50\Omega$), the factor $\sqrt{Z_{C,2}/Z_{C,1}}$ becomes 1.

3. UWB ANTENNA QUALITY MEASURES

The antenna model of Section 2 enables the description of the radiation of arbitrary waveforms like Gaussian pulses or chirps and so forth. The model covers all dispersive effects that result from a particular antenna structure (e.g., the influence of coupled resonators and the related varying group delay due to nonlinear phase response). The influences of frequency-dependent matching and losses are also covered since the feeding network is included in the model. Thus quality measures of the efficiency of a particular more or less dispersive UWB antenna-under-test (AUT) can be derived directly from the antenna's transient response h_n.

In this context, there are two important effects to be distinguished: firstly, the ability of the antenna to effectively transmit and receive power and secondly, the distorting influence on the waveform to be transmitted or received.

3.1. Frequency-domain parameters

As shown in [5, 6, 10], the effective continuous-wave (CW) gain pattern G_{eff} can be computed from the transfer function as follows:

$$G_{\text{eff}}(\omega, \theta, \psi) = \frac{\omega^2}{\pi c_0^2} \left| \vec{H}_n(\omega, \theta, \psi) \right|^2. \tag{11}$$

The IEEE standard antenna gain [11], which excludes the losses due to mismatching, is easily calculated from G_{eff} by accounting for the antenna's input reflection coefficient $S_{11}(\omega)$ (10):

$$G(\omega, \theta, \psi) = \frac{G_{\text{eff}}(\omega, \theta, \psi)}{1 - \left| S_{11}(\omega) \right|^2}. \tag{12}$$

In order to obtain measures for distortion in the frequency domain, the antenna's transfer function for the polarization of interest is denoted as the frequency-dependent complex function $H_{n,\text{copol}}(\omega) = |H_{n,\text{copol}}(\omega)| e^{j\varphi(\omega)}$ with the magnitude $|H_{n,\text{copol}}(\omega)|$ in meter and the phase angle $\varphi(\omega)$ in radians. As known from the theory of filter design [12], the group delay $\tau_g(\omega)$ of a transfer function is defined as

$$\tau_g(\omega) = -\frac{d\varphi(\omega)}{d\omega} = -\frac{d\varphi(f)}{2\pi df}. \tag{13}$$

The group delay is the delay that a portion of the spectral energy at a given angular frequency ω encounters when transmitted through the filter. For minimum distortion, the group delay should be constant within the frequency band of interest. In this case, the phase increases linearly with frequency. The distorting effects can be investigated by introducing a relative group delay:

$$\tau_{g,\text{rel}}(\omega) = \tau_g(\omega) - \tau_{g,\text{mean}}. \tag{14}$$

The frequency-dependent relative group delay $\tau_{g,\text{rel}}(\omega)$ can be reduced to one integral parameter by taking the standard deviation within the frequency band of interest:

$$\tau_{g,\text{RMS}} = \sqrt{\frac{1}{\omega_2 - \omega_1} \int_{\omega_1}^{\omega_2} \tau_{g,\text{rel}}^2(\omega) d\omega}. \tag{15}$$

3.2. Time-domain parameters

The antenna effects on pulse distortion are also to be investigated in the time domain. For the sake of simplification, the formulations are all given for the copolarization. The antenna's transient response will always have no content at $\omega = 0$ according to (4). Therefore, it will contain at least one zero crossing which will not necessarily end the "main" pulse. Common time-domain measures for pulse width and ringing can be applied, despite this, when analyzing the envelope of the analytic response, which is defined in the frequency domain as [13]

$$H_{n,\text{copol}}^{+}(\omega) = \begin{cases} 2H_{n,\text{copol}}(\omega) & \text{for } \omega > 0, \\ 0 & \text{for } \omega \leq 0. \end{cases} \tag{16}$$

The Fourier transform of (16) yields the complex analytical response h_n^+ in the time domain. The relation to the real-valued antenna's transient response is

$$h_{n,\text{copol}}(t) = \Re\{h_{n,\text{copol}}^{+}(t)\}. \tag{17}$$

According to (2), the peak output voltage from an incident waveform depends on the peak value $p(\theta, \psi)$ of the antenna's transient response:

$$p(\theta, \psi) = \max_t \left| h_{n,\text{copol}}^{+}(t, \theta, \psi) \right|. \tag{18}$$

A measure for the linear distortion of the antenna is the envelope width, which is defined as the full width at half maximum (FWHM) of the magnitude of the transient responses envelope:

$$w_{0.5}(\theta, \psi) = t_1 \Big|_{|h_n^+(t_1,\theta,\psi)| = p/2} - t_2 \Big|_{\tau_2 < \tau_1,\, |h_n^+(t_2,\theta,\psi)| = p/2}. \tag{19}$$

The duration of the ringing $\tau_{r,\alpha}$ is defined accordingly as the time until the envelope has fallen from the peak value below a certain lower bound (e.g., below a fraction α of the main peak):

$$\tau_{r,\alpha}(\theta, \psi) = t_\alpha \Big|_{h_n^+(t_\alpha,\theta,\psi) = \alpha p(\theta,\psi)} - t_p \Big|_{t_p < \tau_\alpha \wedge h_n^+(t_p,\theta,\psi) = p(\theta,\psi)}. \tag{20}$$

An integral parameter for the dispersive properties of the antenna in the time domain is the delay spread τ_{DS} of its real valued transient response. The delay spread of a radio channel is calculated from its power delay profile [14], therefore the antenna's delay spread is calculated from the power

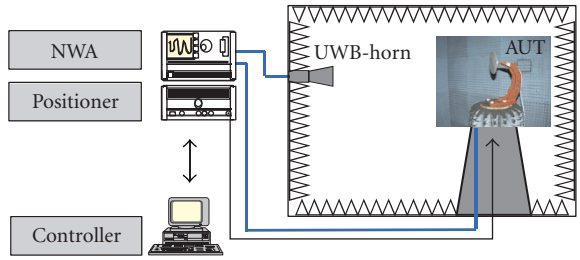

Figure 1: Measurement setup for transmission measurement with the vector network analyzer (VNWA).

related $|h_n|^2$:

$$\tau_{\mathrm{DS}}(\theta,\psi) = \frac{\int_{-\infty}^{\infty} \left(t - \tau_{D,\mathrm{mean}}(\theta,\psi)\right)^2 \left|h_{n,\mathrm{copol}}(t,\theta,\psi)\right|^2 dt}{\int_{-\infty}^{\infty} \left|h_{n,\mathrm{copol}}(t,\theta,\psi)\right|^2 dt} \tag{21}$$

with

$$\tau_{D,\mathrm{mean}}(\theta,\psi) = \frac{\int_{-\infty}^{\infty} t \left|h_{n,\mathrm{copol}}(t,\theta,\psi)\right|^2 dt}{\int_{-\infty}^{\infty} \left|h_{n,\mathrm{copol}}(t,\theta,\psi)\right|^2 dt}. \tag{22}$$

The mean effective G_{mean} in the regarded frequency band can be used as a first estimate for power budget calculations:

$$\begin{aligned} G_{\mathrm{mean,copol}}(\theta,\psi) &= \frac{1}{\omega_2-\omega_1}\int_{\omega_1}^{\omega_2} G_{\mathrm{eff,copol}}(\omega,\theta,\psi)\,d\omega \\ &= \frac{1}{\omega_2-\omega_1}\int_{\omega_1}^{\omega_2} \frac{\omega^2}{\pi c_0^2}\left|H_{n,\mathrm{copol}}(\omega,\theta,\psi)\right|^2 d\omega. \end{aligned} \tag{23}$$

The above procedure can be generalized by weighting the antenna gain with the input signal to be radiated. This can be achieved with the transient effective gain, which is an integral quality measure and evaluates the ability of an antenna to radiate the power of a given waveform $u_{\mathrm{tx}}(t)$:

$$\begin{aligned} g_{T,\mathrm{eff,copol}}(\theta,\psi) &= \frac{\left|\left|h_{n,\mathrm{copol}}(t,\theta,\psi) * du_{\mathrm{tx}}(t)/dt\right|\right|^2}{\left|\left|\sqrt{\pi}c_0 u_{\mathrm{tx}}(t)\right|\right|^2} \\ &= \frac{\left|\left|H_{n,\mathrm{copol}}(\omega,\theta,\psi)\, j\omega U_{\mathrm{tx}}(\omega)\right|\right|^2}{\left|\left|\sqrt{\pi}c_0 U_{\mathrm{tx}}(\omega)\right|\right|^2} \end{aligned} \tag{24}$$

with

$$\left|\left|y(t)\right|\right|^2 = \int_{-\infty}^{\infty} \left|y(t)\right|^2 dt. \tag{25}$$

This power-related definition of the transient gain differs slightly from the one given by Baum in [5] which is Voltage related. If u_t is an ideal bandpass signal with constant spectral density, (24) becomes the mean effective gain G_{mean} in the regarded frequency band as given in (23).

4. MEASUREMENT OF THE TRANSIENT RESPONSE

The frequency-domain measurements presented here have been performed with a HP8530A vector network analyzer and a PHYTRON turn-table positioner supporting the AUT within an anechoic chamber as shown in Figure 1. As a reference antenna, an UWB horn antenna is used. The measurement system is fully computer-controlled. The measurement frequency range is from 400 MHz to 20 GHz (24.5 MHz resolution). A proper calibration has been used in order to eliminate dispersive effects of the connecting cables. The measured S_{21} as the over all transfer function from AUT to reference antenna includes the effects of eventual mismatch at the antenna port. The terminating loads immanent to the measurement system are $Z_{C1} = Z_{C2} = 50\Omega$. According to (9), this yields

$$\begin{aligned} S_{21}(\omega) &= \frac{U_{\mathrm{rx},2}(\omega)}{U_{\mathrm{tx},1}(\omega)} \\ &= H_{n,\mathrm{ref,copol}}(\omega) H_{n,\mathrm{AUT,copol}}(\omega) \frac{j\omega}{2\pi rc} e^{-j\omega r_{12}/c_0}. \end{aligned} \tag{26}$$

With two identical UWB horn antennas, the complex transfer function $H_{\mathrm{ref}}(\omega)$ of the reference horn antenna can be calculated from (26) (see [8]), since the distance r_{12} between the two antennas is known:

$$H_{n,\mathrm{ref,copol}}(\omega) = \sqrt{\frac{2\pi rc}{j\omega} S_{21}(\omega) e^{j\omega r_{12}/c_0}}. \tag{27}$$

In order to obtain physical results, the phase of the transmission coefficient $S_{21}(\omega)$ has to be unwrapped correctly. Thus a proper frequency resolution is needed. With the known reference $H_{n,\mathrm{ref}}(\omega)$, the transfer functions of the AUT is easily calculated solving (26) for $H_{\mathrm{rx,ref}}(\omega)$. This has to be done for all relevant 2D cuts of the antenna radiation pattern at two orthogonal polarizations (co- and cross-polarization). The complex transfer function is obtained for discrete positive frequencies with a resolution $\Delta\omega = 2\pi\Delta f$. It can be transformed into the time domain by inverse discrete Fourier transformation with the appropriate scale factor $1/(N\Delta t)$:

$$h^+_{n,\mathrm{AUT}}(k\Delta t) = \frac{1}{N\Delta t}\sum_{n=0}^{N-1} H^+_{n,\mathrm{AUT}}(n\Delta f) e^{j(2\pi/N)kn}. \tag{28}$$

The result of (28) is a complex discrete-time function with a sampling rate $\Delta t_{\mathrm{raw}} = 1/f_{\max} = 50$ picoseconds. The measured data is complemented by zero padding for 0–400 MHz and 20–200 GHz. This leads to a fine interpolation of the antenna's transient response with an interpolated time resolution of $\Delta t = 5$ picoseconds. Since only the measured positive frequencies are used for the transformation, it results in a time-discrete analytical signal [15]. Its magnitude is referred to as transient response's envelope $|h^+_{n,\mathrm{AUT}}|$. The real part $\Re\{h^+_{n,\mathrm{AUT}}\}$ is taken as a time-discrete estimate for the AUTs transient response h_n similar to (17). It is possible to double the time resolution of the measured transient response by combining real and imaginary part of $h^+_{n,\mathrm{AUT}}$ as shown in [16].

For the evaluation of u_{rx} according to (10), together with the measured h^+_{AUT}, the derivative of the simulated time-domain excitation voltage has to be converted first into a discrete-time analytical signal by the discrete Hilbert transform [15]. The estimate for the output voltage of the

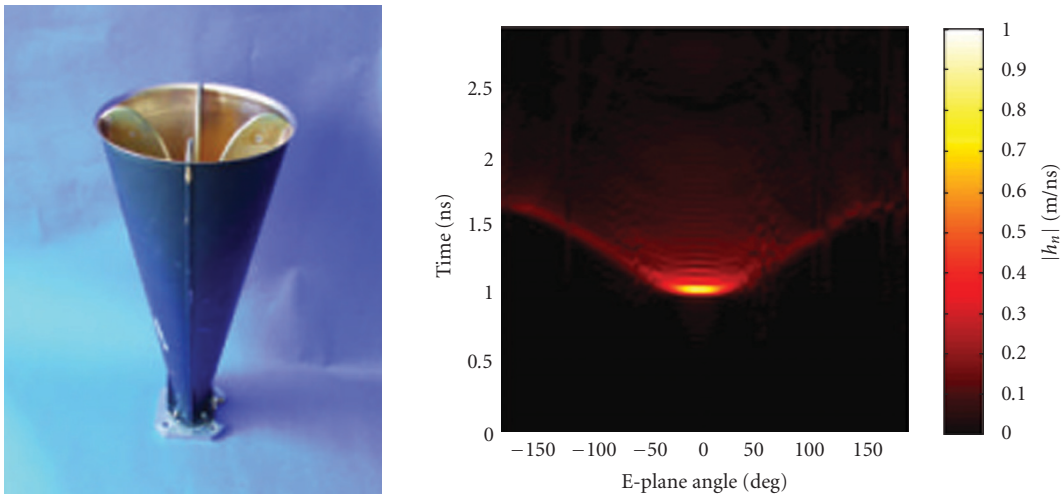

(a) (b)

FIGURE 2: (a) Quad-ridged horn. (b) Measurement of the transient response envelope versus angle and time for the E-plane and copolarization.

receiving antenna is then computed in the frequency domain by multiplying the discrete frequency vectors of the antenna transfer functions with the exciting signals according to (9). This procedure makes use of the cyclic convolution properties of the discrete Fourier transform (DFT) and it has to be ensured, that the length of the time vector is sufficient in order to avoid ambiguities. The transfer functions of the connecting cables are measured separately and inserted in the simulation. A verification of this method with the short-pulse time-domain measurements is given in [17].

4.1. Measurement results

The transient response of the employed reference horn antenna (quad-ridged horn, 2–20 GHz) in the E-plane shows a sharp and high peak in the main lobe as can be seen from Figure 2. The horn antenna (model A6100, EM systems) is used as a fixed receiving antenna in the measurement setup. It is 300 mm long and the diameter of the aperture is 140 mm. It exhibits an effective gain from 5 to 19 dBi, which increases from 2 to 20 GHz. The half-power beamwidth is decreasing from 70° to 13° over the specified frequency range. Two identical horn antennas are available for calibration. The measured h_n exhibits a high and sharp peak with $p = 0.93$ m/ns and $w_{0.5} = 65$ picoseconds. That is expected since the horn structure is nonresonant and provides a smooth transition from the transmission line to the free space.

The absolute time delay of the maximum in Figure 2 exhibits a sinusoidal dependence over the rotation angle ψ. The explanation is, that the center of rotation did not exactly coincide with the apparent phase center of the antenna [3], which can be called also center of radiation. This can be partly corrected by estimating the center of radiation [19] and reprocessing or repeating the measurement with an improved antenna position. However, the time-domain quality measures (Section 3) are not affected by this effect because they do not refer to absolute delays and are calculated independently for every direction.

The transient response of a Vivaldi antenna, which has been designed for the frequency range 3.1 GHz–10.6 GHz and which was presented in [18], shows also a relatively sharp peak (Figure 3). The antenna has significantly less gain than the horn antenna, which is mainly due to its smaller aperture (50 mm tapered-slot width). Therefore, the peak magnitude of its transient response is $p_{\max,\text{Vivaldi}} = 0.35$ m/ns lower than that of the horn.

Obviously, the effort in aligning the antenna on the turn table becomes less tedious if the antenna size is small. Therefore, it is assumed that the center of radiation lies within the physical structure of the antenna. However, the measurement of the Vivaldi antenna with the size 78 mm × 75 mm, which is small compared to the horn, exhibits also an angle dependent h_n with sinusoidal components. For the side and backward directions, the antenna's transient response $|h_n(t, |\psi| > 50°)|$ shows two peaks. For those directions, a unique center of radiation cannot be defined. The two peaks can be explained by the structure of the antenna: the first backward peak is due to the feeding network and the second one emerges from reflections at the Vivaldi antenna's aperture. This illustrates how the analysis of the antenna's transient response gives valuable insights to the antenna designer. In Figure 4, the structure and the transient response for a logarithmic-periodic dipole array (LPDA) is shown. In contrast to the horn and the Vivaldi antenna the broadband behavior of the LPDA is due to coupled resonances. This results in a long duration of the transient response $w_{0.5} = 785$ picoseconds and a strongly reduced peak value $p = 0.13$ m/ns.

5. PATTERNS OF THE QUALITY MEASURES

The measurements of transient responses for three different antennas are presented here for a UWB horn antenna (2–20 GHz), for a planar Vivaldi antenna (3.1–10.6 GHz), and for a planar LPDA (3.1–10.6 GHz). The planar Vivaldi antenna and the LPDA have been presented in [18].

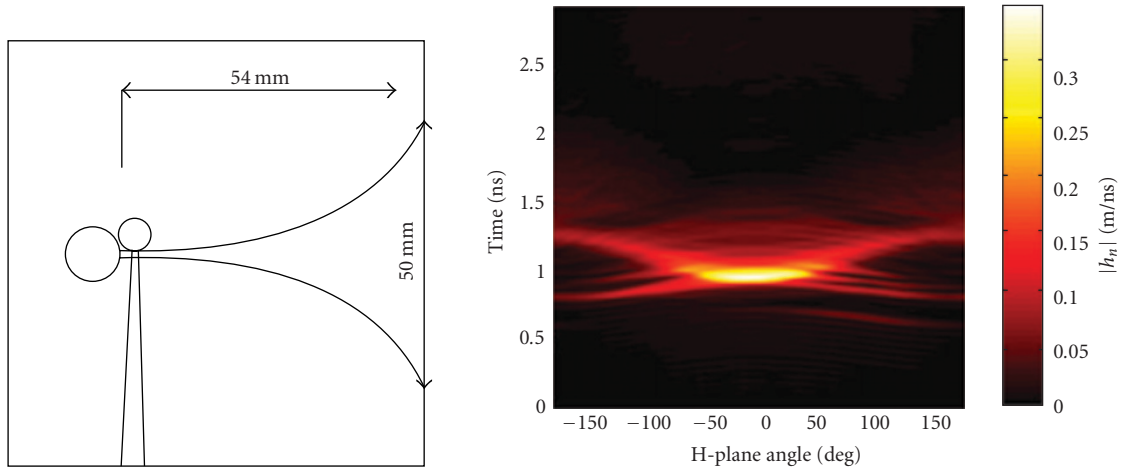

(a) (b)

Figure 3: (a) Structure of Vivaldi antenna [18]. (b) Measurement of the transient response envelope versus angle and time for the H-plane and copolarization.

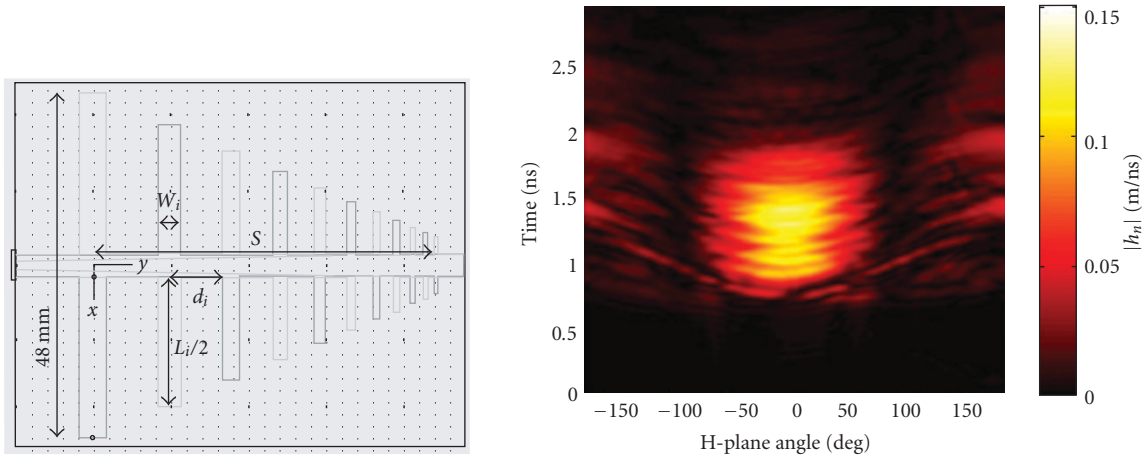

(a) (b)

Figure 4: (a) Structure of LPDA [18]. (b) Measurement of the transient response envelope versus angle and time for the E-plane and copolarization.

All antennas are linearly polarized. The graphs presented below show the directional characteristics for the time-domain quality measures (Section 3) in the E-plane of each antenna. The frequency-domain parameters like gain and group delay are discussed in more detail in [20, 21].

5.1. Horn antenna

The transient response of the horn antenna shows a sharp and high peak value p in the main beam direction ($\psi = 0°$). As can be seen from Figure 5b, p decreases fast for off-boresight angles. The half-power (-3 dB) width of the peak value pattern $p(\omega)$ is 31°. The half-voltage (-6 dB) width is 45°. The time dependence for the main beam direction is shown in Figure 6a. The envelope of the transient response gives a good impression where the main signal parts are concentrated. Some high-frequency oscillations ($f = 20$ GHz) are overlaid to the signal. This is due to the sharp edge of the measurements of the rectangular window in the frequency domain. Therefore, this effect is easily reduced using additional filtering. It has to be emphasized that the derived quality measures can only be compared if measurement bandwidth and additional filtering are equal for the measured transient responses. The directional dependence of the transient response's peak width $w_{0.5}(\psi)$ and the ringing $\tau_{r,\alpha}(\psi)$ in the E-plane are shown in Figure 6b. The lower bound α for the definition of the ringing $\tau_{r,\alpha}$ has to be chosen very carefully according to the noise floor of the measurement. In order to compare the ringing of antennas with different gains under the constraint of a constant noise floor, the fraction α has been chosen to be $\alpha = 0.22(-13\,\text{dB})$.

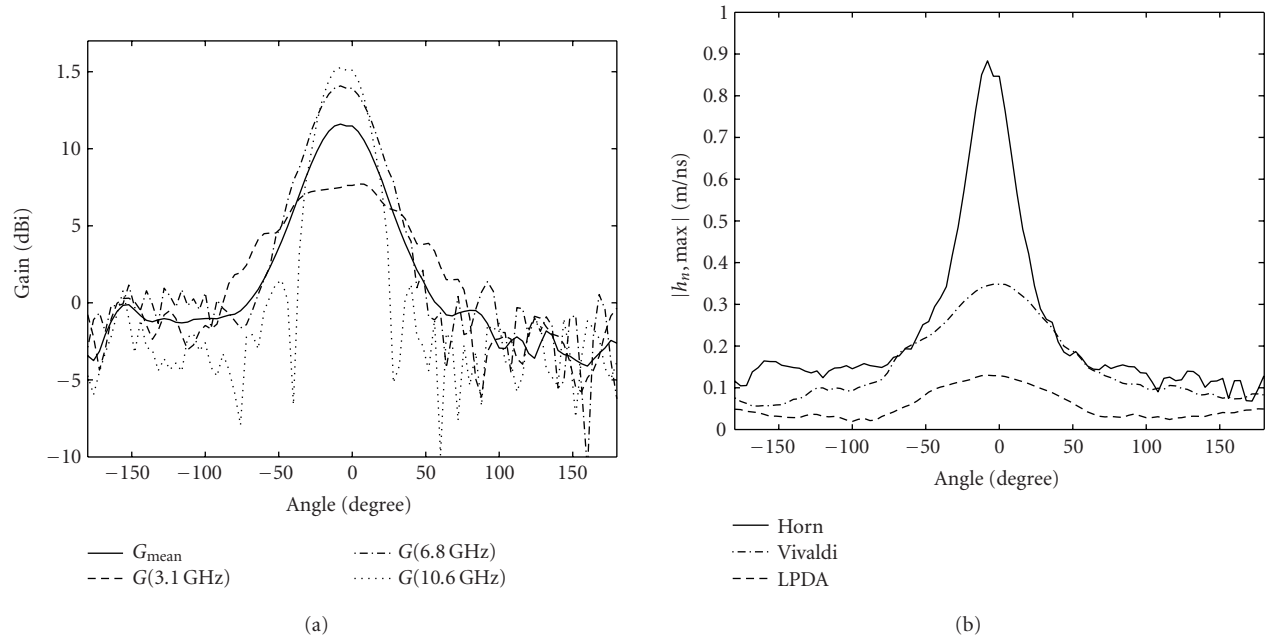

FIGURE 5: (a) Mean-effective gain G_{mean} (integrated from 3.1–10.6 GHz) and gain G for selected frequencies (E-plane, measurement frequency range 0.4–20 GHz). (b) Comparison of peak magnitudes of the transient response for horn, Vivaldi, and LPDA (E-plane in each case).

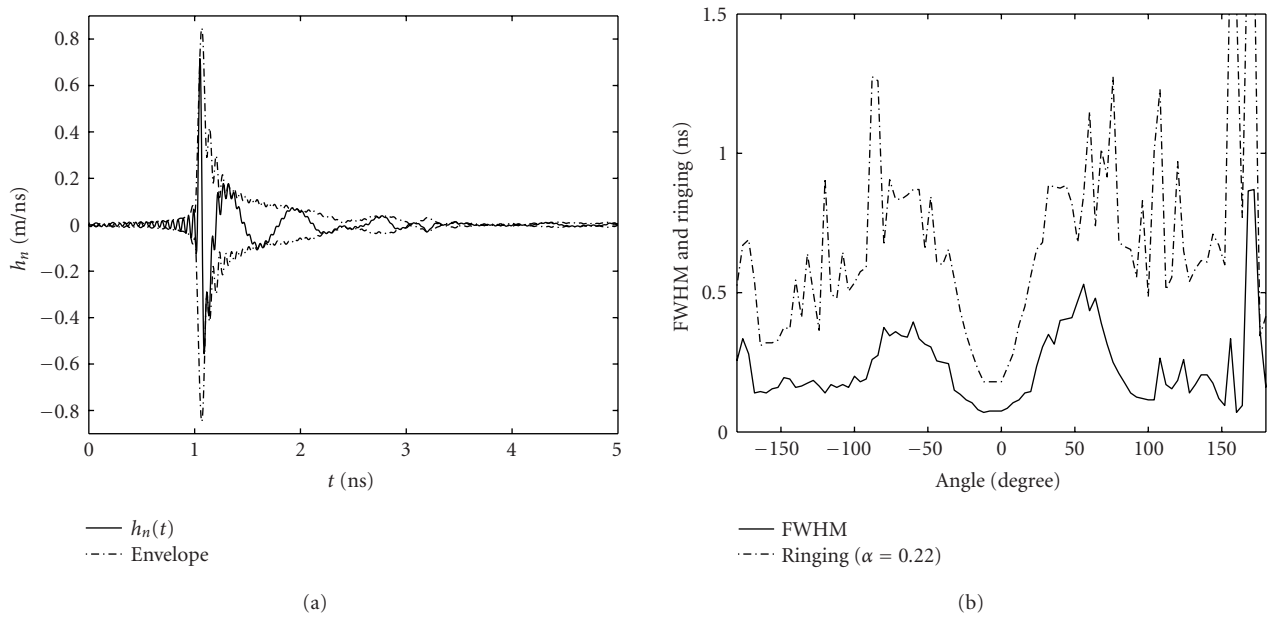

FIGURE 6: (a) Transient response in direction 0° for the horn antenna (E-plane). (b) FWHM and duration of the ringing for the horn antenna (E-plane).

The minimum ringing is $\tau_{r,\alpha} = 355$ picoseconds for the main beam direction ($\psi = 0°$). It rises when turning the antenna. This can be explained by the fact that the peak magnitude of the transient response decreases outside the main lobe of the antenna, whereas the unwanted long-lasting, lower frequent oscillations are radiated quite omnidirectional. The FWHM of the main peak shows only weak variations within the main lobe of the antenna. In Figure 5a, the mean-effective gain of the antenna according to (23) is shown. It is compared to the effective gain patterns for selected frequencies within the FCC frequency range. Due to the averaging over frequency, the nodes and side lobes of the narrowband gain patterns are smoothed. The half-power beamwidth of the mean-effective gain pattern is 33° and agrees therefore very well with that 31° of the peak value pattern $p(\psi)$ although they are not identical. Note that the peak value pattern in Figure 5b is

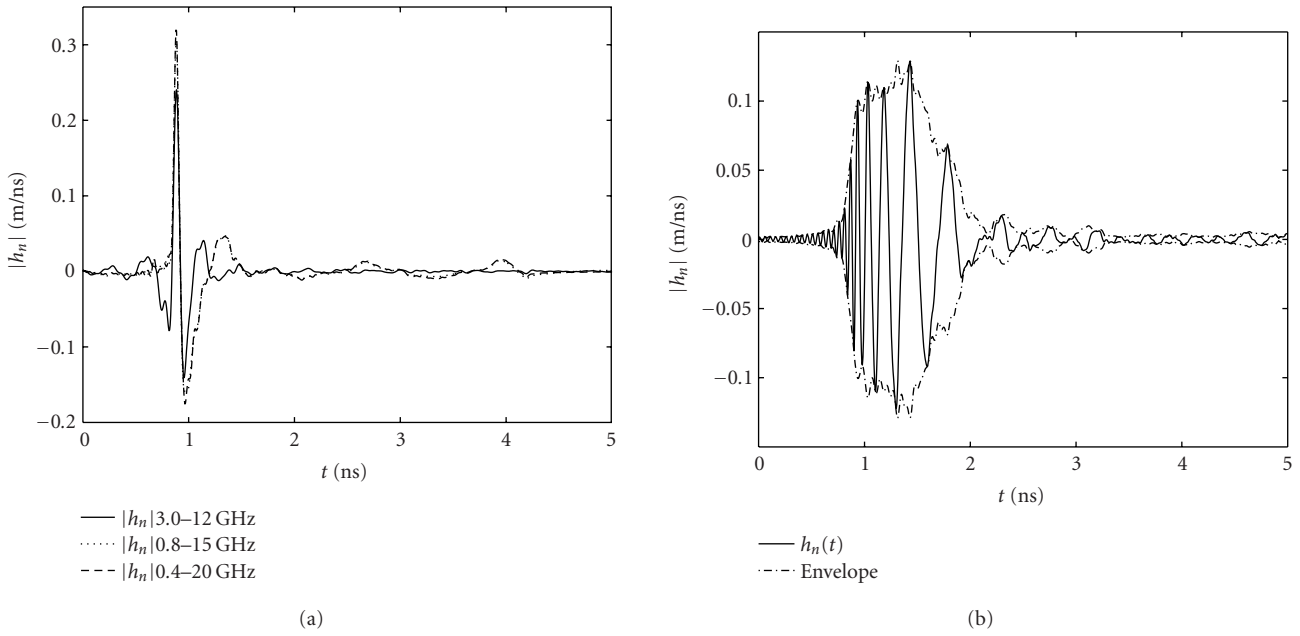

Figure 7: (a) Transient response of Vivaldi antenna in the main beam direction for different measurement bandwidths. (b) Transient response of LPDA (measurement bandwidth 20 GHz).

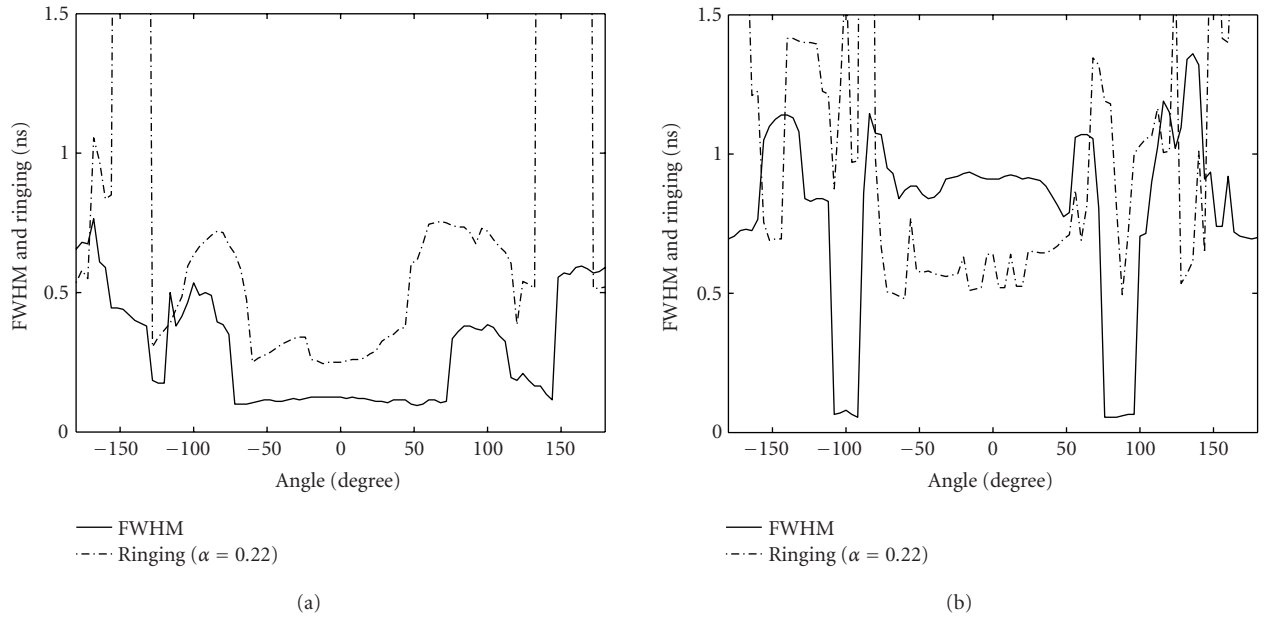

Figure 8: FWHM and duration of the ringing (E-plane, measurement frequency range 0.4–20 GHz): (a) Vivaldi antenna; (b) LPDA.

given in a linear scale, whereas the gain patterns in Figure 5a are given in the dB scale.

5.2. Vivaldi antenna and LPDA

The transient response of the Vivaldi antenna shows like the horn antenna a sharp peak in the time domain and low ringing (cf. Figures 7 and 8). Figure 7 shows the transient response of the Vivaldi antenna for different measurement bandwidths. The original measurement bandwidth 0.4–20 GHz is reduced to 0.8–15 GHz and 3–12 GHz. The first reduction has almost no influence on the shape of the transient response. The maximum peak is reduced from $p_{0.4\text{–}20\,\text{GHz}} = 0.3448$ m/ns to $p_{0.8\text{–}15\,\text{GHz}} = 0.3410$ m/ns and the FWHM is increased from $p_{0.5,0.4\text{–}20\,\text{GHz}} = 115$ picoseconds to $p_{0.5,0.4\text{–}20\,\text{GHz}} = 130$ picoseconds. This shows that the Vivaldi antenna operates mainly in frequencies below 15 GHz. The further reduction of the bandwidth has a significant impact on the resulting transient response: the peak

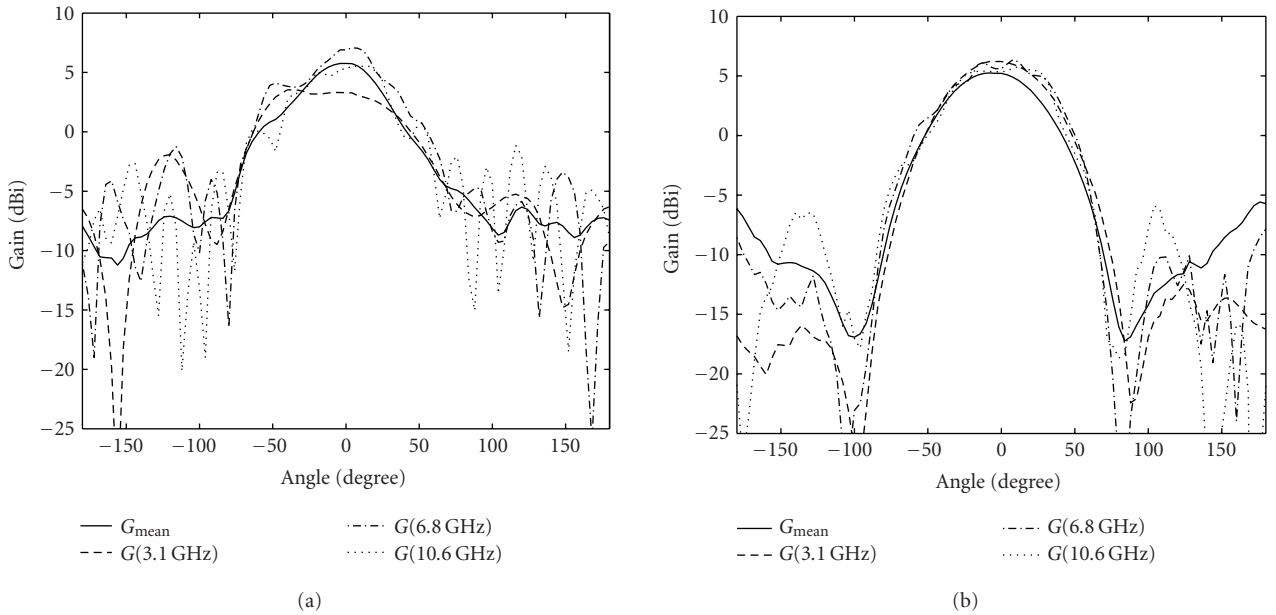

Figure 9: Mean-effective gain G_{mean} (integrated from 3.1–10.6 GHz) and gain G for selected frequencies (E-plane, measurement frequency range 0.4–20 GHz): (a) Vivaldi antenna; (b) LPDA.

Table 1: Measurement results of the quality measures for some antennas (main beam direction).

	p	$w_{0.5}$	$\tau_{r,0.22}$	G_{mean}	G(3.1 GHz)	G(6.85 GHz)	G(10.6 GHz)
Broadband	0.93 m/ns	65 ps	355 ps	12.2 dB	7.7 dBi	13.9 dBi	15.2 dBi
Horn Vivaldi	0.34 m/ns	115 ps	475 ps	5.7 dB	3.3 dBi	6.7 dBi	4.6 dBi
Antenna LPDA	0.13 m/ns	785 ps	440 ps	5.3 dB	6.4 dBi	6.4 dBi	4.8 dBi

magnitude is reduced to $p_{0.8\text{–}15\,\text{GHz}} = 0.2313$ m/ns, the FWHM is increased to $p_{0.5,0.4\text{–}20\,\text{GHz}} = 150$ picosecond, but the ringing is reduced from $\tau_{r,0.22,0.4\text{–}20\,\text{GHz}} = 475$ picoseconds to $\tau_{r,0.22,3\text{–}12\,\text{GHz}} = 265$ picoseconds. This is because the ringing spectral components below 3 GHz are suppressed. These emerge from a resonance of the antenna structure at 2.1 GHz, which radiates omnidirectionally. Figure 8a shows the FWHM $w_{0.5}(\psi)$ and the ringing $\tau_{r,0.22}(\psi)$ of the Vivaldi for the measurement bandwidth 0.4–20 GHz. The peak width and the ringing are quite constant over the main lobe, which is broader than that of the horn. In the azimuth (E-plane) directions of $\psi = +150^\circ$ and $\psi = -150^\circ$, the peak magnitude of the transient response $p(\psi = \pm 150^\circ)$ is very weak. For those angles, the lower bound of the ringing definition conflicts with the noise floor of the measurement (approx. 0.02 m/ns). Therefore, the ringing results are not valid for those directions.

The LPDA exhibits a different behavior than the horn or the Vivaldi. That is due to the fact, that the LPDA is a resonant structure with coupled dipole elements [18, 19]. As can be seen from Figure 7b, its transient responses envelope does not have a sharp peak. It rather consists of an oscillation with decreasing frequency, because the dipoles with higher resonance frequencies are excited earlier than the larger dipoles.

Therefore, the peak magnitude of the transient responses envelope is only 37% of the Vivaldi antenna's peak magnitude. However, the mean gain of LPDA (Figure 9b) and Vivaldi (Figure 9a) are approximately equal ($G_{\text{mean,Vivaldi}} = 5.7$ dBi, $G_{\text{mean,LPDA}} = 5.3$ dBi). The ringing in main beam direction (Figure 8b) is lower than the FWHM, because they are defined on the transient responses envelope, which is quite symmetric to the time of its peak value. Therefore, the time from envelopes peak value to the lower bound is shorter than the FWHM. The boresight values of the envelope peak $p(\psi = 0^\circ)$, FWHM $w_{0.5}(\psi = 0^\circ)$, ringing $t_{r,0.22}(\psi = 0^\circ)$, and gains $G_{\text{eff,mean}}(\psi = 0^\circ)$, $G(\psi = 0^\circ, f)$ are summarized for the different antennas in Table 1.

6. CONCLUSIONS

Since an antenna is a linear time-invariant (LTI) system, it can be fully described by the directional antenna transfer function in both, the frequency or the time domain. The particular representation of the antenna transfer function yields the full information in each domain. However, some effects like ringing, maximum-pulse amplitudes, group-delay characteristics, or frequency-selective behavior are investigated best in the domain in which they are defined. Therefore, one measurement in either the frequency or the time domain will provide this information by applying adequate signal processing for the transformation between both domains. The measurement in the frequency domain exhibits standardized

and easy calibration methods and has a dynamic range above 90 dB. The shape of the antenna's directional transient response is directly connected to the physical structure, which will be optimized not only for perfect impulse radiation but also for small size and low cost. The tradeoffs between these optimization goals can be visualized by analyzing the transient response and its derived quality measures as shown above. Furthermore, the quantified influence of the antennas on the UWB transmission can lead to a joint optimization of modulation schemes and antenna properties.

REFERENCES

[1] Federal Communications Commission (FCC), "Revision of Part 15 of the Commission's Rules Regarding Ultra Wideband Transmission Systems," *First Report and Order*, ET Docket 98-153, FCC 02-48; Adopted: February 2002; Released: April 2002.

[2] M. Thumm, W. Wiesbeck, and S. Kern, *Hochfrequenzmeßtechnik*, B.G. Teubner, Stuttgart, Germany, 1998.

[3] C. A. Balanis, *Antenna Theory: Analysis and Design*, Wiley & Sons, New York, NY, USA, 1996.

[4] H. H. Meinke and F. W. Gundlach, *Taschenbuch der Hochfrequenztechnik: Grundlagen, Komponenten, Systeme,* edited by K. Lange and K.-H. Löcherer, Springer, Berlin, Germany, 1992.

[5] C. E. Baum, "General properties of antennas," *Sensor and Simulation Notes*, note 330, Directed Energy Directorate, Air Force Research Laboratory, Kirtland, NM, USA, 1991.

[6] E. G. Farr and C. E. Baum, "Extending the definitions of antenna gain and radiation pattern into the time domain," *Sensor and Simulation Notes*, note 350, Directed Energy Directorate, Air Force Research Laboratory, Kirtland, NM, USA, 1992.

[7] L. Bowen, E. Farr, and W. Prather, "A collapsible impulse radiating antenna," in *Proc. Ultra-Wideband Short-Pulse Conference*, pp. 299–309, Tel Aviv, Israel, June 2000.

[8] B. Scheers, M. Acheroy, and A. V. Vorst, "Time-domain simulation and characterisation of TEM horns using a normalised impulse response," *IEE Proceedings-Microwaves, Antennas and Propagation*, vol. 147, no. 6, pp. 463–468, 2000.

[9] M. Kanda, "Time domain sensors for radiated impulsive measurements," *IEEE Trans. Antennas Propagat.*, vol. 31, no. 3, pp. 438–444, 1983.

[10] J. Kunisch and J. Pamp, "UWB radio channel modeling considerations," in *Proc. International Conference on Electromagnetics in Advanced Applications (ICEAA '03)*, pp. 277–284, Torino, Italy, September 2003.

[11] IEEE, "IEEE standard definition of trans. for antennas," IEEE Std. 145-1993, Institute for Electrical and Electronics Engineering, New York, NY, USA, March 1993.

[12] A. V. Oppenheim, *Discrete-Time Signal Processing*, Prentice Hall, Englewood Cliffs, NJ, USA, 1989.

[13] J. G. Proakis, *Digital Communications*, McGraw-Hill, New York, NY, USA, 3rd edition, 1995.

[14] N. Geng and W. Wiesbeck, *Planungsmethoden für die Mobilkommunikation*, Springer, Heidelberg, Germany, 1998.

[15] D. Iverson, "Extracting real samples from complex sampled data," *IEEE Electronics Letters*, vol. 27, no. 21, pp. 1976–1978, 1991.

[16] S. L. Marple Jr., "Computing the discrete-time "analytic" signal via FFT," *IEEE Transactions on Signal Processing*, vol. 47, no. 9, pp. 2600–2603, 1999.

[17] W. Sörgel, F. Pivit, and W. Wiesbeck, "Comparison of frequency domain and time domain measurement procedures for ultra wideband antennas," in *Proc. 25th Annual Meeting and Symposium of the Antenna and Measurement Techniques Association (AMTA '03)*, pp. 72–76, Irvine, Calif, USA, October 2003.

[18] W. Sörgel, C. Waldschmidt, and W. Wiesbeck, "Transient responses of a Vivaldi antenna and a logarithmic periodic dipole array for ultra wideband communication," in *Proc. IEEE Antennas and Propagation Society International Symposium*, vol. 3, pp. 592–595, Columbus, Ohio, USA, June 2003.

[19] H. Ebert, J. Sachs, R. Zetik, and P. Rauschenbach, "Characterising of impulse radiating antennas," in *Proc. 48th Internationales Wissenschaftliches Kolloquium*, p. 20, Technische Universität Ilmenau, Ilmenau, Germany, September 2003.

[20] W. Sörgel, C. Waldschmidt, and W. Wiesbeck, "Antenna characterization for ultra wideband communications," in *Proc. International Workshop on Ultra Wideband Systems (IWUWBS '03)*, Oulu, Finland, June 2003.

[21] W. Sörgel, C. Waldschmidt, and W. Wiesbeck, "Electromagnetic characterization of ultra wideband antennas," in *Electromagnetics in a Complex World*, I. M. Pinto, V. Galdi, and L. B. Felsen, Eds., pp. 225–234, Springer, Berlin, Germany, 2004.

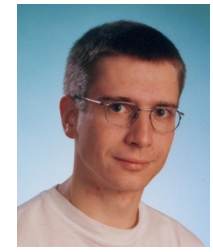

Werner Sörgel was born in Karlsruhe, Germany, in 1974. After his military service, he studied electrical engineering at the University of Karlsruhe. He received the Dipl.-Ing. degree in electrical engineering (M.S.E.E.) in 2001. Since May 2001, he has been with the Institut für Höchstfrequenztechnik und Elektronik (IHE), Universität Karlsruhe (TH), Germany, as a Research Associate. He is currently working towards the Dr.-Ing. (Ph.D.E.E.) degree. His present research topics are mainly focused on ultra-wideband (UWB) antenna design and channel characterization. He has been awarded with the 2003 Student Paper Award of the Antenna Measurement Techniques Association. He is a Student Member of the IEEE.

Werner Wiesbeck received the Dipl.-Ing. (M.S.E.E.) and the Dr.-Ing. (Ph.D.E.E.) degrees from the Technical University, Munich, in 1969 and 1972, respectively. From 1972 to 1983, he was with AEG-Telefunken in various positions including Head of R&D Microwave Division, and Marketing Director Receiver and Direction Finder Division, Ulm. Since 1983, he has been the Director of the Institut für Höchstfrequenztechnik und Elektronik (IHE), Universität Karlsruhe (TH). Research topics include radar, remote sensing, wireless communication, and antennas. He is a Member of the IEEE GRS-S AdCom (1992–2000), Chairman of the GRS-S Awards Committee (1994–1998, 2002), Executive Vice-President of the IEEE GRS-S (1998–1999), President of the IEEE GRS-S (2000–2001), Associate Editor of the IEEE-AP Transactions (1996–1999), and past and present Treasurer of the IEEE German Section (1987–1996, 2003–2005). He has been the General Chairman of the 1988 Heinrich Hertz Centennial Symposium, and the 1993 Conference on Microwaves and Optics (MIOP '93). He received a number of awards, lately the IEEE Millennium Award, and the IEEE GRS Distinguished Achievement Award. He is a Fellow of IEEE, a Member of the Heidelberger Academy of Sciences, and a Member of acatech (German Academy of Engineering and Technology).